

Multispectral imaging and hyperspectral scanning of the first dissection of core 73002: Preliminary results

Lingzhi SUN^{1*}, Paul G. LUCEY¹, Abigail FLOM¹, Chiara FERRARI-WONG¹, Ryan A. ZEIGLER², Juliane GROSS^{2,3}, Noah E. PETRO⁴, Charles K. SHEARER⁵, Francis M. McCUBBIN², and The ANGSA Science Team

¹Department of Earth Sciences, Hawai'i Institute of Geophysics and Planetology, University of Hawai'i at Manoa, 1680 East-West Rd, Honolulu, Hawai'i 96822, USA

²Astromaterials Acquisition and Curation Office, NASA Johnson Space Center, Houston, Texas 77058, USA

³Department of Earth & Planetary Sciences, Rutgers State University of New Jersey, Piscataway, New Jersey 08854, USA

⁴Solar System Exploration Division, NASA Goddard Space Flight Center, Greenbelt, Maryland 20771, USA

⁵Institute of Meteoritics, Department of Earth and Planetary Sciences, University of New Mexico, Albuquerque, New Mexico 87131, USA

*Corresponding author. E-mail: lzsun@higp.hawaii.edu

(Received 20 January 2021; revision accepted 10 June 2021)

Abstract—We measured the multispectral images and a hyperspectral profile during the first dissection pass of core 73002, and here, we present preliminary results. Both multispectral images and hyperspectral data show systematic darkening and reddening from bottom to top of the core, indicating an increasing maturity from the subsurface to surface soils. Our estimated FeO and TiO₂ abundances are 9 (± 1) wt% and 1.8 (± 0.5) wt%, and their homogeneous distributions imply no compositional stratigraphy was sampled by core 73002. The in situ regolith reworking depth is about 14 cm as inferred from the optical maturity (OMAT) profile, corresponding to a time range of about 61 million years. Mineralogy and Mg# (molar Mg/[Mg+Fe]) calculated using hyperspectral data and radiative transfer modeling show as expected the core is dominated by plagioclase and low-Ca pyroxene, and the average Mg# is 61 (± 10). Our work shows that spectroscopy has a great potential to be applied in the preliminary examination of future extraterrestrial samples from outside of the glovebox.

KEY POINTS

- We observed systematic darkening and reddening from bottom to top of the core 73002.
- OMAT profile indicates an in situ regolith reworking depth of 14 cm.
- Major minerals of the core are plagioclase and low-Ca pyroxene.

INTRODUCTION

The double drive tube 73001/2 was sampled at Station 3 during extravehicular activity (EVA) 2 of the Apollo 17 mission, located on the Light Mantle deposit in the southwest of the Taurus–Littrow valley, near the rim of the 620 m diameter Lara Crater and the 10 m

diameter Ballet Crater (Butler 1973) (Fig. 1). The Light Mantle may be the result of one or more landslides from the South Massif (Schmitt et al. 2017), and the latest landslide was inferred to be caused by secondary impacts from Tycho (Arvidson et al. 1976; Lucchitta 1977) or the movement of the Lee-Lincoln faults (Schmitt et al. 2017). Petrological study of soil samples collected from the Light Mantle shows the presence of noritic breccias, melt rocks, and anorthositic rocks (Bence et al. 1974).

The double drive tube is up to 60 cm in length and 4 cm in diameter (Zeigler et al. 2020). Core 73002 is the upper segment, and it sampled 23 cm in depth (LSPET 1973). X-ray scans show that core 73002 mainly consists of soil, but several rock fragments can also be observed, and these fragments tend to concentrate at the lower

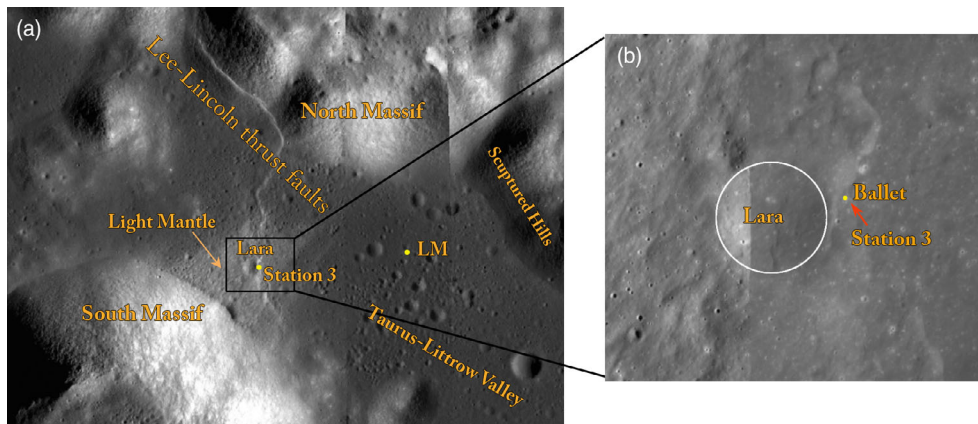


Fig. 1. a) Geologic context of the sampling location of the double drive tube 73001/2, which was sampled at Station 3. b) A zoomed-in image of the frame in (a), showing that Station 3 is located near craters Lara and Ballet. The base maps are from the Lunar Reconnaissance Orbiter Camera (LROC), Wide Angle Camera (WAC), and Narrow Angle Camera (NAC) [NASA/GSFC/ASU]. (Color figure can be viewed at wileyonlinelibrary.com.)

part of the core (LSPET 1973; Zeigler et al. 2020). However, this distribution may not be representative of the local regolith, since a nearby trench (samples 73220, 73240, 73260, 73280) of the upper 10–15 cm regolith shows no clear indication of increasing rock fragments with depth (Butler 1973).

On November 5, 2019, the Apollo Next Generation Sample Analysis (ANGSA) team opened core 73002, beginning to examine the first of the two pristine core samples. As part of basic characterization and preliminary examination of the 73002 core, spectral imaging and hyperspectral scans of the core are being carried out by the University of Hawai'i, supported by the science team of ANGSA and the Apollo curatorial facility (Shearer et al. 2020). In this article, we present some preliminary results of multispectral imaging and hyperspectral profile obtained during the first dissection pass of core 73002. Furthermore, we demonstrate the feasibility of spectroscopic measurements on pristine samples from outside the pristine glovebox environment. This work represents an important step forward for nondestructive analysis of pristine samples where the analysis does not compromise the pristine environment in which the sample is contained.

METHODS

To establish measurement methodologies, we carried out preliminary multispectral imaging and a hyperspectral profile during the first dissection pass of the core using existing instrumentation, including a multispectral camera covering 400–1000 nm and a hyperspectral point spectrometer covering 400–2500 nm. The core is in a borosilicate glass-topped glovebox

purged with dry nitrogen (details on the composition of the dry nitrogen are provided in McCubbin et al. 2019). We are only able to obtain soil spectra in the wavelength range of 400–2500 nm, which is the spectral transmission range of the borosilicate glass. During the measurement, spectral disturbance caused by borosilicate was not observed. The schematic diagram of the spectroscopy system is shown in Fig. 2. Both instruments are installed on the frame on top of the glovebox, and the light source is shared by the multispectral imaging camera and hyperspectrometer. Both the multispectral images and hyperspectral data were acquired with a 15° incidence angle, 10° emission angle, and a 25° phase angle in plane. A Teflon standard that is cross calibrated to the spectral reflectance standard Spectralon was used as the “reflectance standard.” The “dark” images contain background signal of the spectrometer and the environment, and they were measured for each scan at each wavelength and then subtracted from both raw and standard spectral data. Then, the reflectance data were calculated by ratioing the “dark removed” spectral data and the reflectance standard.

The multispectral imaging system uses an Orion StarShoot G3 deep space monochrome imaging camera, with a Thorlabs Inc. six-position motorized filter wheel, and six narrow band interference filters from Edmund Optics. The filters cover six wavelengths: 415, 570, 750, 900, 950, and 990 nm (Table 1), sharing some of the bands used by the Clementine Ultraviolet/Visible (UVVIS) camera, the Lunar Reconnaissance Orbiter Camera Wide Angle Camera (LROC WAC), and the KAGUYA Multiband Imager (MI) spectrometer. The multispectral imaging system images the core at 60 µm/pixel spatial resolution, and the field of view (FOV) is

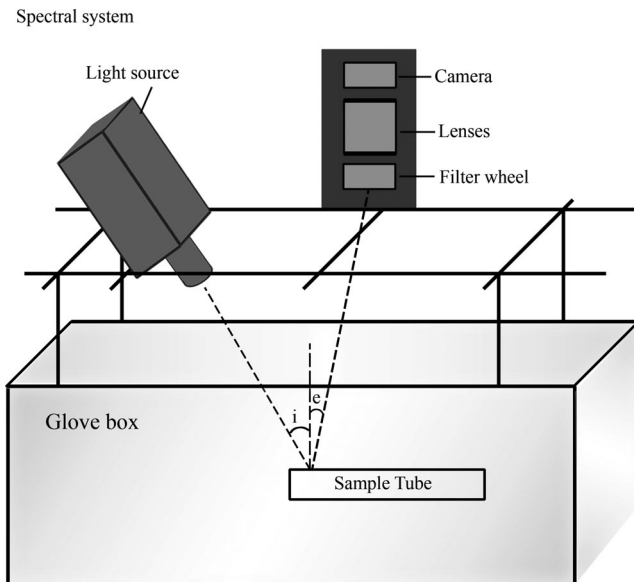


Fig. 2. The spectral measurement system, consisting of a light source and spectrometer, is located on a frame above the glovebox (size not to scale). The multispectral imaging set includes light source, camera, lenses, and filter wheel. For the hyperspectral measurements, we replaced the multispectral set with an ASD probing fiber.

about 47×36 mm. However, the available spectral illuminator did not cover the entire core width, and the illuminated area was a roughly 30 mm diameter circle within the image frame (shown in Fig. 3), and the detected FOV of preliminary measured images is a 30 mm circle.

The hyperspectral data were acquired by an analytical spectral devices (ASD-FR) spectrometer, with its wavelengths covering 400–2500 nm at 10 nm spectral resolution, substantially overlapping remote sensing spectral data from Moon Mineralogy Mapper (M^3) on board Chandrayaan-1, the Spectral Profiler (SP) on board Kaguya, and the large lunar soil spectral data sets measured at RELAB (Reflectance Experiment Laboratory). During the preliminary measurements, spectra of 17 spots were measured at 10 mm increments along the center of the core, and 10 spectra were

collected at each spot. To suppress possible artificial effects and increase the signal-to-noise ratio, we averaged 10 reflectance spectra for each spot and acquired a profile consisting of 17 spectra along the core. The hyperspectral data were not usable beyond 1700 nm due to low signal-to-noise ratio from a combination of low spectral irradiance from the illuminator and low sensitivity of the spectrometer at longer wavelengths; thus, the wavelength range we used for analysis is 500–1700 nm. A new illuminator will be applied in future measurements, which allows us to obtain spectral data from 400 to 2500 nm.

RESULTS AND DISCUSSIONS

Geologic Context of Station 3

FeO concentration and degree of space weathering optical maturity (OMAT) distributions for the Taurus-Littrow valley were mapped using Kaguya MI data and the algorithm from Lemelin et al. (2015), shown in Fig. 4. Station 3 is located on the Light Mantle, and the FeO content is about 8.5 wt%, which is close to the average of Light Mantle and South Massif materials (Fig. 4a) (Jolliff 1999). The optical maturity of the Light Mantle is higher than the basaltic materials within the valley, indicating that the Light Mantle soils are less mature (Fig. 4b).

There are some soil samples collected from Station 3 near the double drive core, including one soil containing dust abraded off rocks (73211) and four trench soils from the upper 10–15 cm of the regolith (73221, 73241, 73261, and 73281), which can be used as reference samples for core 73002. We list the mineralogy, compositions, and Is/FeO of these reference soils in Table 2. The mineralogy is similar among these soils, with their average plagioclase abundance being 68 vol%. The Mg# (molar $\text{Mg}/[\text{Mg}+\text{Fe}]$) of soils varies within a narrow range (64–70), and the average value is around 67. All the soils have moderate FeO and low TiO_2 content, and the average abundance for FeO and TiO_2 is 8.8 and 1.8 wt%, respectively. Maturity index Is/FeO measured by Morris (1978b) using FMR

Table 1. Instrumental parameters of the multispectral imaging and hyperspectral system during preliminary measurements.

Parameters	Multispectral imaging system	Hyperspectral system
Wavelengths (nm)	415, 570, 750, 900, 950, 990	500–1700
Viewing geometry	$i = 15^\circ, e = 10^\circ$	$i = 15^\circ, e = 10^\circ$
Spectral resolution	(FWHM) 10 nm	10 nm
Spatial resolution	60 $\mu\text{m}/\text{pixel}$	10 mm/pixel
FOV/sampling intervals	30 mm circle	10 mm
Coverage	About 75% of the core (Fig. 3)	One profile along center (Fig. 5a)

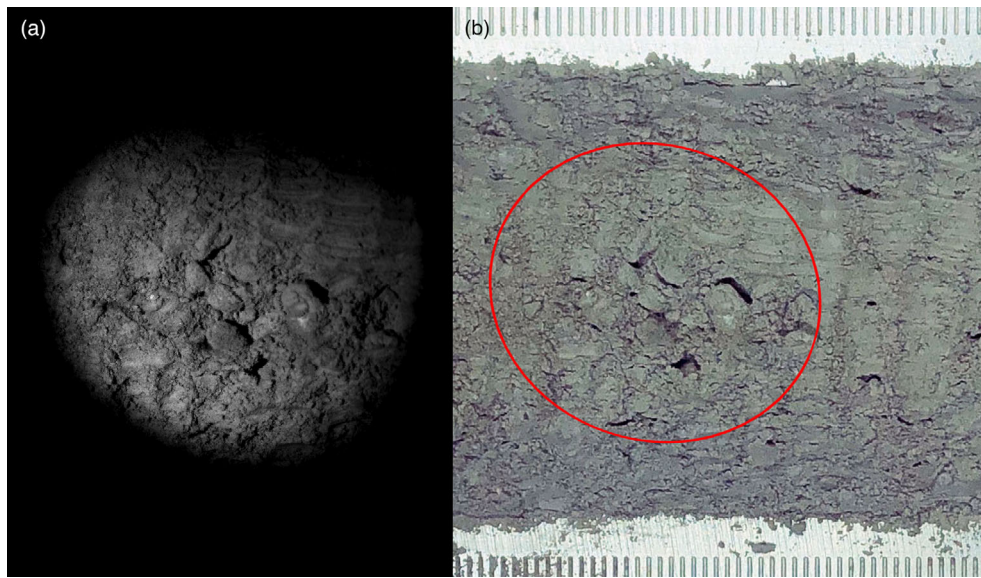


Fig. 3. a) One image frame at 570 nm of the multispectral imaging scans, and the same area is circled in (b), which is a zoomed-in photo of the core. More than 75% in width of the core is illuminated and captured by the multispectral imager. (Color figure can be viewed at [wileyonlinelibrary.com](#).)

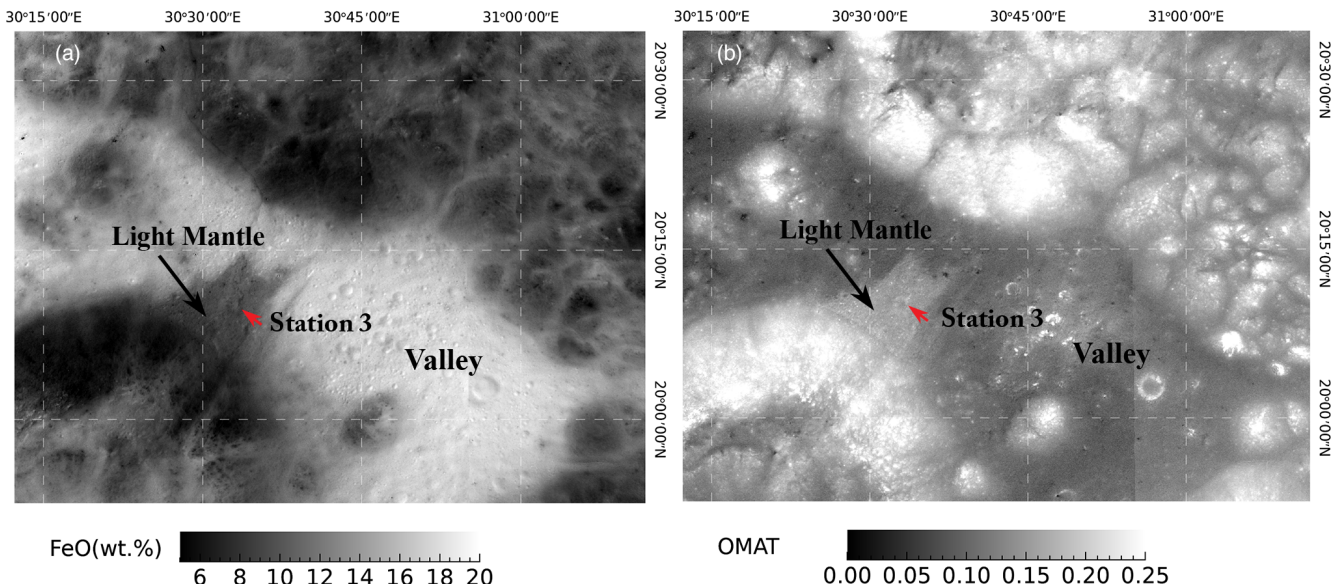


Fig. 4. a) FeO and (b) OMAT maps of the Apollo 17 landing area derived from Kaguya Multiband Imager data and the algorithm from Lemelin et al. (2015). Red arrows indicate location of Station 3. (Color figure can be viewed at [wileyonlinelibrary.com](#).)

suggests most of the Station 3 soils are submature (Is/FeO = 34–45), and 73241 is the only immature soil (Is/FeO = 18).

Multispectral Imaging Scans

The multispectral images were measured in December of 2019, during the first dissection pass of core 73002. The original sampling depth of core 73002

is estimated at 23 cm (LSPET 1973), and it is compressed to 18.5 cm after being extruded from the tube (Zeigler et al. 2020). We took 72 images (12 scans at 6 wavelengths) along the core, and made a mosaic shown in Figs. 5b and 5c. Reflectance at 570 nm (Fig. 5b) shows a systematic darkening effect from the bottom to top of the core, which can be attributed to space weathering. We also produced a color ratio image (Fig. 5c) using similar bands that were applied in the

Table 2. Compositional information of soils collected at Station 3.

Sample	Oliv ^a	LCP ^a	HCP ^a	Plag ^a	Mg# ^b	FeO ^b	TiO ₂ ^b	Is/FeO ^c	Sample info ^d
73211	12.7	13.3	5.4	68.5	—	8.93 ^e	—	39	Dust abraded off rocks
73221	12.1	16.3	5.4	66.2	64.1	8.85	1.86	43	Trench soils, surface
73241	11.6	16.6	5.0	66.8	69.8	8.45	1.73	18	Trench soils, surface
73261	12.3	14.9	6.4	66.4	68.5	8.86	1.9	45	Trench soils, subsurface
73281	12.8	6.9	9.0	71.4	66.5	8.82	1.76	34	Trench soils, subsurface

^aMineral modal abundances (in vol%) measured by Taylor et al. (2019) with X-ray diffraction.

^bFeO and TiO₂ contents (in wt%) measured by Rose et al. (1974) with microchemical techniques. Mg# = molar Mg/(Mg+Fe).

^cIs/FeO measured by Morris (1978b).

^dSampling information from Butler (1973).

^eFeO content (in wt%) measured by Korotev and Kremser (1992) with instrumental neutron activation analysis.

Clementine UVVIS images (Fischer and Pieters 1996), and the three channels are red = 750/415 nm, green = 750/950 nm, and blue = 415/750 nm. The red channel is sensitive to the maturity of soils, green channel is sensitive to the abundance of FeO, and blue channel is sensitive to the abundance of TiO₂. From Figs. 5a and 5c, systematic reddening trend from bottom to top of the core can be observed, suggesting an increase in maturity. The light shade in blue from Fig. 5c indicates low TiO₂ content for soils within the core.

We used a 15° incidence angle when acquiring the images, resulting in frequent shadows. To suppress the influence of shadows, we averaged the reflectance across the width of the core (Fig. 5) and plotted 950/750 nm ratio versus 750 nm reflectance in Fig. 6a. On the one hand, variation along the FeO axis is small, implying a relatively homogeneous compositional distribution within the core. On the other hand, an obvious darkening and reddening trend can be observed along the OMAT axis, indicating a gradient in maturity. Similarly, the ratio of 415/750 nm is plotted versus 750 nm reflectance in Fig. 6b, which can be used to determine the TiO₂ abundance.

FeO and TiO₂ Abundances

To quantify the FeO abundances for the core, a dark and red endmember is found at $x_{0\text{Fe}} = 0.08$, $y_{0\text{Fe}} = 1.15$ in Fig. 6a, and Equation (1) is used to calculate the FeO content (Lucey et al. 2000). The profile and map of FeO content are shown in Figs. 7a and 7b. In spite of the spikes caused by shadowing, the FeO content of the whole core shows a relatively constant distribution. Statistically, the peak concentration of FeO content is about 9 wt%, consistent with those measured from the trench soils (Table 2); standard deviation of FeO content is 1.0 wt%, suggesting a uniform FeO distribution within the core.

$$\text{FeO}(\text{wt}\%) = 19 \times \left[-\arctan \left(\frac{R_{950}/R_{750} - y_{0\text{Fe}}}{R_{750} - x_{0\text{Fe}}} \right) \right] \quad (1)$$

To estimate the abundance of TiO₂, we adopted the TiO₂ origin ($x_{0\text{Ti}} = 0.0$, $y_{0\text{Ti}} = 0.42$) from Lucey et al. (2000) (Fig. 6b), and used Equation (2) to estimate the TiO₂ content. The profile and map of TiO₂ distribution within the core are shown in Figs. 7c and 7d. Statistically, the peak value of TiO₂ abundance is near 1.8 wt%, consistent with the trench soils (Table 2); the standard deviation is about 0.5 wt%.

$$\text{TiO}_2(\text{wt}\%) = 3.708 \times \left[\arctan \left(\frac{R_{415}/R_{750} - y_{0\text{Ti}}}{R_{750} - x_{0\text{Ti}}} \right) \right]^{5.979} + 1.5 \quad (2)$$

Both the estimated FeO and TiO₂ contents show a homogeneous compositional distribution along the core, indicating that the compositional stratigraphy of the local regolith may be not sampled by core 73002.

Maturity Profile and Regolith Reworking Depth

OMAT is calculated using the Euclidean distance to the endmember ($x_{0\text{Fe}}$, $y_{0\text{Fe}}$) from Fig. 6a (Lucey et al. 2000), and lower OMAT value corresponds to higher soil maturity. The OMAT profile and map of the core are shown in Figs. 8a and 8b, and the spikes in OMAT profile are more likely due to illumination and/or topography of the dissected surface. Lucey et al. (2014) mentioned that OMAT is sensitive to topography because its calculation requires reflectance. OMAT decreases from bottom to surface of the core, showing a profile of increasing degree of space weathering. Reference soils collected near the surface (Table 2) are mostly submature based on their Is/FeO values, implying the maturity of core soils may range from immature (bottom) to submature (surface),

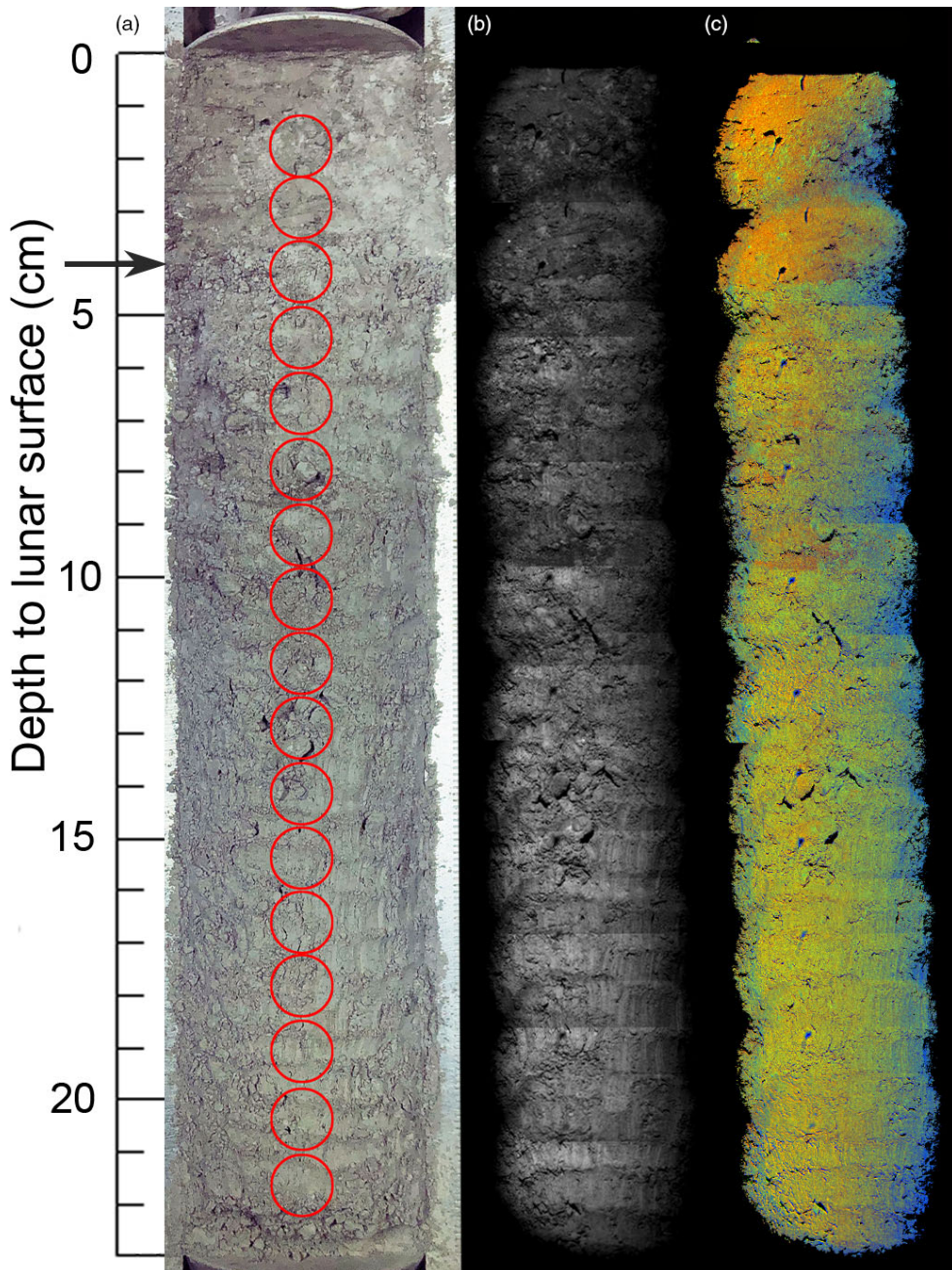


Fig. 5. Core 73002 images taken during the first dissection, and the depth to lunar surface is labeled on the left. a) Photograph of the core taken by Dr. Paul Lucey, with red circles indicating hyperspectral profile footprints. The arrow points to the dissection progress. b) Core mosaic in 570 nm reflectance. c) A color ratio image of the core mosaic, red = 750/415 nm, green = 750/950 nm, and blue = 415/750 nm. (Color figure can be viewed at wileyonlinelibrary.com.)

corresponding to a 60% increase in OMAT from bottom to top of the core.

Space weathering can produce nano- and micro-phase Fe on the exposed surface of the Moon, and these metallic Fe phases dominate the spectral darkening and reddening effect (Keller et al. 1998; Noble et al. 2001, 2007), causing a higher maturity in

surface soils. These surface metallic Fe phases can also mix into subsurface soils through impacts, and constant impacts can generate a relatively high maturity zone near the surface, and this mixing progress is interpreted as *in situ* regolith reworking or gardening (McKay et al. 1977). This regolith reworking zone has been found in Apollo 15, 16, and 17 deep drill cores by previous

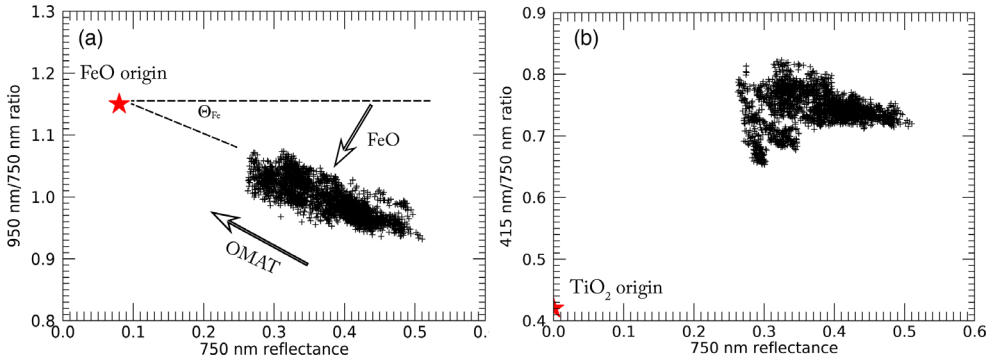


Fig. 6. a) 950 nm/750 nm ratio versus 750 nm reflectance along the core, (b) 415 nm/750 nm ratio versus 750 nm reflectance along the core. To avoid the influence of shadows, the reflectances are averaged along the horizontal direction of the core. (Color figure can be viewed at [wileyonlinelibrary.com](#).)

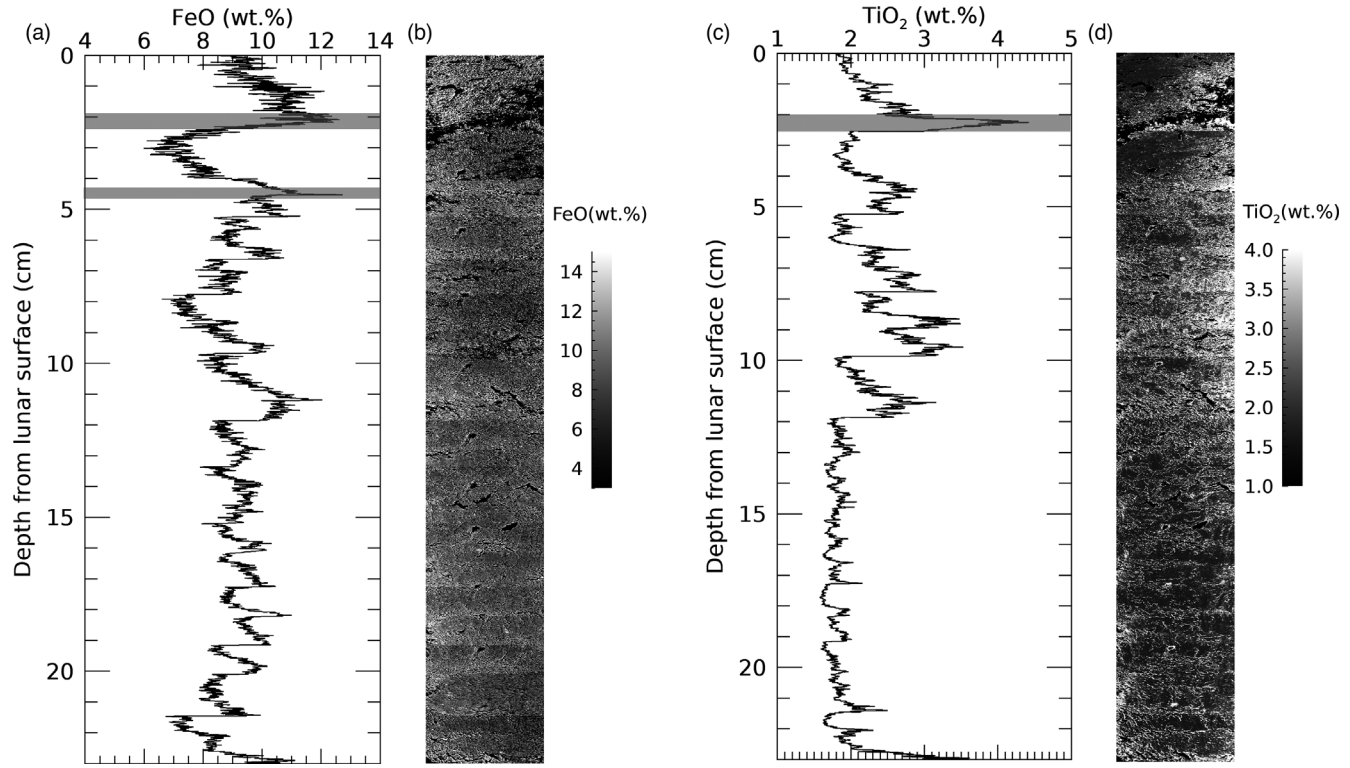


Fig. 7. a) FeO profile along the core, (b) FeO map of the core, (c) TiO₂ profile along the core, and (d) TiO₂ map of the core. Spikes colored in gray in (a) and (c) are likely due to shadows.

workers, for example, Heiken et al. (1976), McKay et al. (1977, 1978), and Morris (1978a).

In terms of core 73002, we also find a relatively high maturity zone within the top 14 cm of the regolith, which exhibits lower OMAT values compared to the lower part of the core (Fig. 8a); therefore, the possible in situ regolith reworking depth is estimated at about 14 cm. Morris (1978a) found that the depth of in situ regolith reworking is associated with time, and they derived a relationship between regolith reworking depth

and time by summarizing data from several Apollo deep drill cores:

$$D_R = 2.2(t)^{0.45} \quad (3)$$

where D_R is the regolith reworking depth in centimeters and t is time in million years. Based on this equation, it takes about 61 Myr to generate the 14 cm higher maturity zone within core 73002.

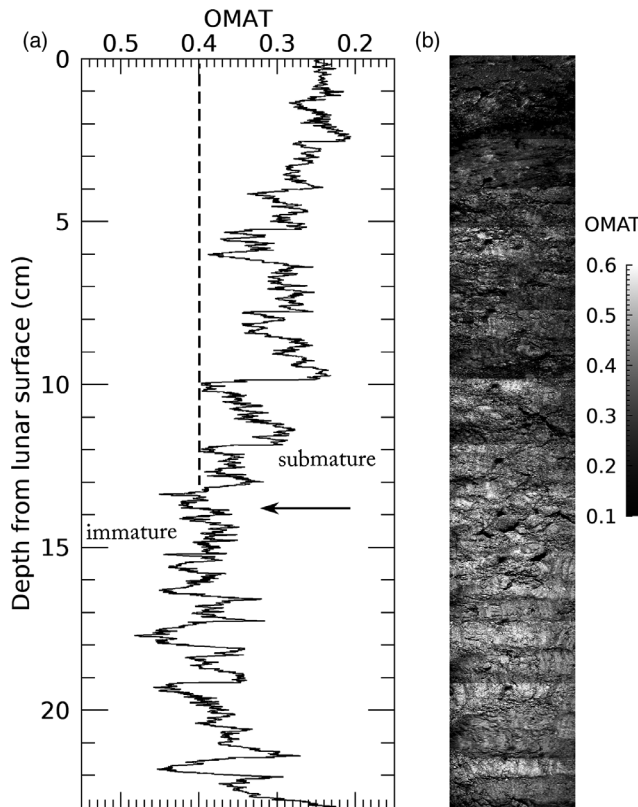


Fig. 8. a) OMAT profile (horizontally averaged) along the core, and the arrow indicates the regolith reworking depth at about 14 cm. b) OMAT map of the whole core.

The homogeneous composition within the core indicates the regolith reworking zone may be due to some small impacts that occurred on the Light Mantle, and we infer that the ejecta of the nearest craters Lara and Ballet may have been emplaced at Station 3.

Hyperspectral Profile

Footprints of the hyperspectral profile are shown in Fig. 5a, with seventeen 10 mm diameter spots measured. The hyperspectral reflectance is shown in Fig. 9, and we use colors to show different depth from the lunar surface. Reflectance spectra show a systematic darkening from bottom to top of the core (Fig. 9a), and a systematic reddening in spectral slope is obvious when normalizing reflectance spectra to 750 nm (Fig. 9b), indicating an increasing maturity from bottom to top of core, and this is consistent with the multispectral imaging results. The continuum removed spectra do not show obvious weakening of absorption band depth near one micron as expected (Fischer and Pieters 1996) (Fig. 9c), and this might be due to the high feldspathic composition of the soils or the influence of heterogeneous grain size variation within the core.

Sun and Lucey (2021) developed a mineral and chemistry unmixing model using radiative transfer theory, and by applying this model to the 17 ASD spectra, we derive the modal abundances of olivine, low-Ca pyroxene (LCP), high-Ca pyroxene (HCP), and plagioclase, as well as Mg# of the core. We plot the mineral modes derived by the Sun and Lucey (2021) model and those of Station 3 soils measured by XRD (Table 2) (Taylor et al. 2019) on the classification diagram of Stöffler et al. (1980) in Fig. 10. The mineralogy of core soils is dominated by plagioclase and LCP, and their modal mineral abundances are consistent with the result of Station 3 trench soils. Sun et al. (2021) reported the mineralogy for 43 Apollo 17 sampling stations using Kaguya MI data and the algorithm from Lemelin et al. (2015), and their results indicate the major mineralogy for South Massif and most of the landslide soils includes plagioclase and LCP, consistent with our results derived from the core. The modeled average Mg# of the 17 spectra is 61 (± 10), which is consistent with that of the trench soils collected at Station 3 (Mg# = 67, Table 2).

CONCLUSIONS

We report the preliminary results of the spectral imaging and hyperspectral profile measured during the first dissection pass of core 73002. Both multispectral imaging and hyperspectral data show systematic spectral darkening and reddening due to space weathering, indicating an increasing maturity profile from bottom to top of the core.

We calculated the FeO and TiO₂ distributions within the core using the color ratio plot and multispectral image, and FeO and TiO₂ concentrates around 9 (± 1) wt% and 1.8 (± 0.5) wt%, respectively. Our estimated FeO and TiO₂ contents both show homogeneous distributions within the core, implying that compositional stratigraphy may be not sampled by core 73002.

We derived an OMAT profile along the core from the color ratio plot and multispectral image, and the OMAT variation is consistent with increasing maturity from bottom to top of the core. A relatively high maturity zone was found within the core, indicating a vertical regolith reworking depth of 14 cm, which corresponds to about 61 Myr in time based on the equation of Morris (1978a).

The major minerals of the core are plagioclase and low-Ca pyroxene based on radiative transfer modeling, and the average Mg# is around 61 (± 10), consistent with those of Station 3 soils measured by XRD (Taylor et al. 2019).

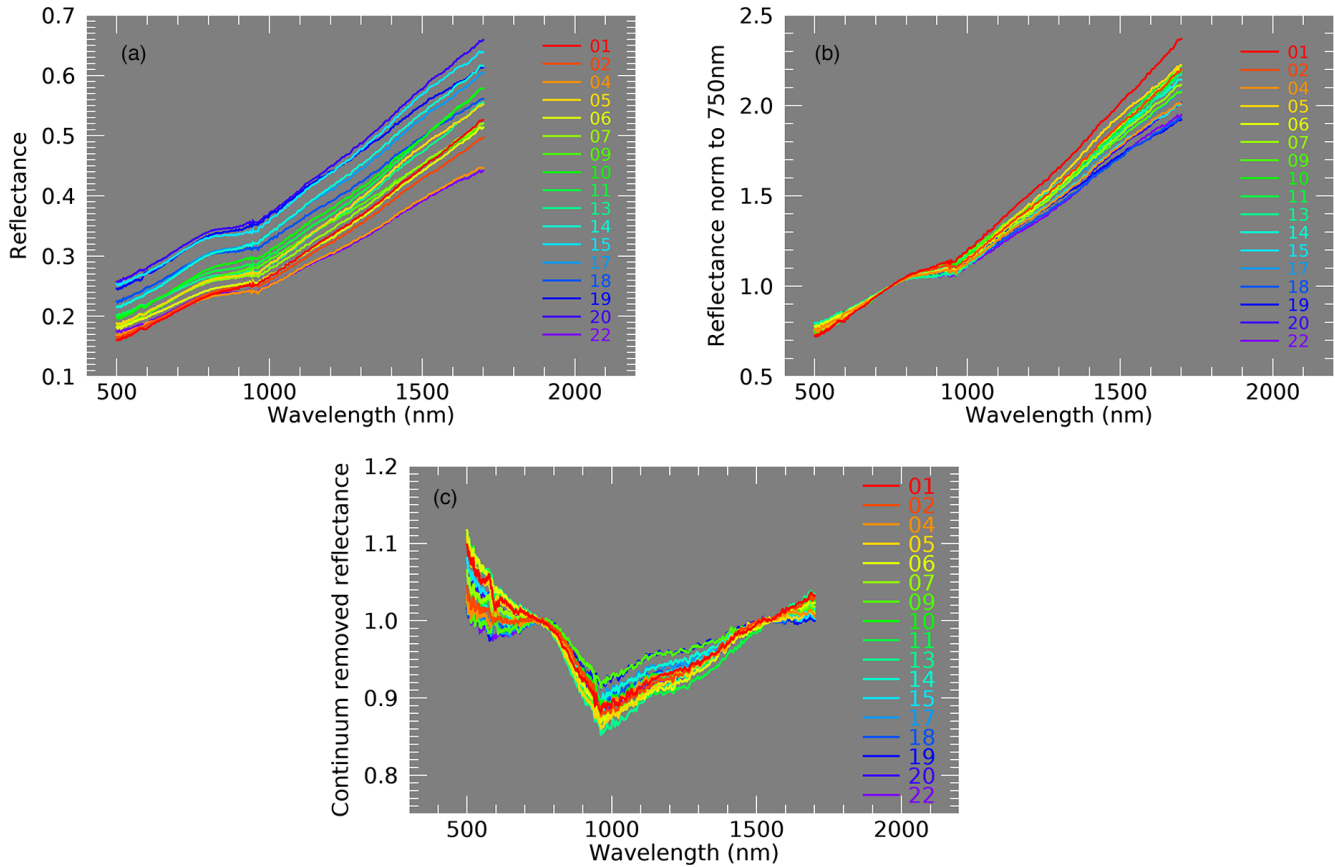


Fig. 9. Hyperspectral profile of the red circles in Fig. 5a, and the depths (in centimeters) to lunar surface are labeled with color. a) Reflectance spectra along the core, showing systematic darkening from bottom to top. b) Reflectance normalized to 750 nm, showing a reddening trend in spectral slope from bottom to top of the core. c) Continuum removed reflectance, and absorption depths at one micron do not vary a lot with sampling depth. (Color figure can be viewed at [wileyonlinelibrary.com](#).)

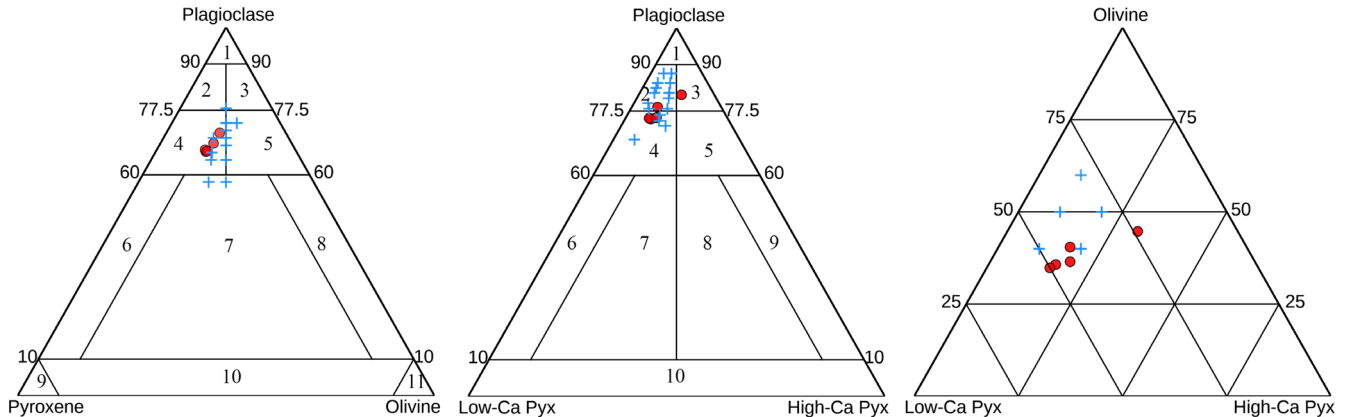


Fig. 10. Mineral modal abundances plotted over the ternary diagram (Stöffler et al. 1980). Note that the use of this diagram is to show the mineral modal abundances rather than rock types. Blue crosses are derived from radiative transfer modeling using the hyperspectral profile of the core, and red dots are from Station 3 soils measured using XRD by Taylor et al. (2019). (Color figure can be viewed at [wileyonlinelibrary.com](#).)

Our spectral records of the core contribute to the documentation of Apollo core samples and provide ground truth in both composition/mineral unmixing and space weathering for remote sensing studies.

In this article, we have shown that spectroscopy can measure the composition and mineralogy for lunar samples that were returned from the Apollo era. Preliminary examinations of post-Apollo samples, for

example, the Artemis samples, in studying the water content and major mineralogy of the lunar south polar region (Gilmour et al. 2020; Mitchell et al. 2020), can benefit from this convenient and nondestructive technique.

FUTURE WORK

Preliminary multispectral imaging scans did not cover the whole core width due to the limitation of the light source. We are completing a custom illuminator that provides illumination of the full width of the core for imaging measurements. During the operational measurements, the whole core will be illuminated and captured by the camera. Hyperspectral profiles will be obtained at 1 mm spatial resolution and 5 mm sampling distance during the operational spectral measurement to provide hyperspectral data throughout the whole core volume.

The use of the 15° incident angle and 25° in plane phase angle in the preliminary data resulted in substantial shadowing at the 100 µm scale; thus, the preliminary data spectral imaging data set will be confined to spectral ratios lacking pixel level photometric correction. To mitigate this, the operational data will be obtained with a zero degree incidence angle to minimize shadowing, and a viewing angle of 15°. We are also completing a new illuminator specifically for the hyperspectral data that will allow us to observe at zero phase angle and eliminate any issues with topographic shading.

In the present study, we demonstrate the usefulness of spectroscopic measurements on pristine samples from outside the pristine glovebox environment. All the spectroscopic data reported here were collected through the borosilicate glass on top of the glovebox cabinet at the Apollo curatorial facility at Johnson Space Center. Although this setup limits the detection range of spectroscopy to visible and near infrared wavelengths, important insights can be gained through such analyses during the basic characterization and preliminary examination portions of pristine sample investigations. The successful demonstration of these measurements lends credence to the application of spectroscopic measurements to pristine samples in containment for future sample return missions (McCubbin et al. 2019), including OSIRIS-REx, Artemis, and Mars Sample Return. Once the core dissection reaches the bottom layer, the core will be moved outside of the pristine sample handling cabinet, making it available for inspection at longer wavelengths. We plan to collect hyperspectral data from 0.5 to 14 µm at 10 mm spatial resolution for this final layer of the core after it is removed from the pristine glovebox and before the final layer is preserved in epoxy.

AUTHOR CONTRIBUTIONS

Lingzhi Sun was involved in conceptualization; formal analysis; writing—original draft; writing—review and editing. Paul G. Lucey was involved in conceptualization; methodology; data curation (lead); writing—review and editing. Abigail Flom and Chiara Ferrari-Wong were involved in data curation. Ryan A. Zeigler and Juliane Gross were involved in data curation (supporting); writing—review and editing. Charles K. Shearer and Francis M. McCubbin were involved in project administration; writing—review and editing. The ANGSA Science Team and Noah E. Petro were involved in writing—review and editing.

Acknowledgments—We thank Dr. Edward Cloutis and the anonymous reviewer for their constructive comments. This work was supported by the NASA Apollo Next Generation Sample Analysis Program (ANGSA). We thank Dr. Emily Costello for useful discussions about regolith reworking.

Data Availability Statement—The mineral modal abundances for reference soils can be found at: <https://odr.io/lunar-regolith-xrd>.

Editorial Handling—Dr. Edward Cloutis

REFERENCES

- Arvidson R., Drozd R., Guinness E., Hohenberg C., Morgan C., Morrison R., and Oberbeck V. 1976. Cosmic ray exposure ages of Apollo 17 samples and the age of Tycho. *Proceedings, 7th Lunar Science Conference*. pp. 2817–2832.
- Bence A., Delano J., Papike J., and Cameron K. 1974. Petrology of the highlands massifs at Taurus-Littrow—An analysis of the 2–4 mm soil fraction. *Proceedings, 5th Lunar Science Conference*. pp. 785–827.
- Butler P. 1973. *Lunar sample information catalog, Apollo 17*. Houston, Texas: Lyndon B. Johnson Space Center.
- Fischer E. M. and Pieters C. M. 1996. Composition and exposure age of the Apollo 16 Cayley and Descartes regions from Clementine data: Normalizing the optical effects of space weathering. *Journal of Geophysical Research: Planets* 101:2225–2234.
- Gilmour C., Gawronska A., Barrett N., Boazman S., Halim S., McCanaan K., Satyakumar A. V., Shah J., and Kring D. A. 2020. Artemis 2024: Potential EVA targets at the lunar south pole (abstract #1482). *51st Lunar Science Conference*. CD-ROM.
- Heiken G., Morris R., McKay D., and Fruland R. 1976. Petrographic and ferromagnetic resonance studies of the Apollo 15 deep drill core. *Proceedings, 7th Lunar Science Conference*. pp. 93–111.
- Jolliff B. L. 1999. Clementine UV-VIS multispectral data and the Apollo 17 landing site: What can we tell and how well? *Journal of Geophysical Research: Planets* 104:14,123–14,148.

- Keller L. P., Wentworth S. J., and McKay D. S. 1998. Space weathering: Reflectance spectroscopy and tem analysis of individual lunar soil grains (abstract #1762). 29th Lunar and Planetary Science Conference. CD-ROM.
- Korotev R. L. and Kremser D. T. 1992. Compositional variations in Apollo 17 soils and their relationship to the geology of the Taurus-Littrow site. Proceedings, 23rd Lunar and Planetary Science Conference. pp. 275–301.
- Lemelin M., Lucey P. G., Song E., and Taylor G. J. 2015. Lunar central peak mineralogy and iron content using the Kaguya Multiband Imager: Reassessment of the compositional structure of the lunar crust. *Journal of Geophysical Research: Planets* 120:869–887.
- LSPET. 1973. Preliminary examination of lunar samples. *Apollo 17: Preliminary Science Report*, NASA SP-330.
- Lucchitta B. K. 1977. Crater clusters and light mantle at the Apollo 17 site; a result of secondary impact from Tycho. *Icarus* 30:80–96.
- Lucey P. G., Blewett D. T., and Jolliff B. L. 2000. Lunar iron and titanium abundance algorithms based on final processing of clementine ultraviolet-visible images. *Journal of Geophysical Research: Planets* 105:20,297–20,305.
- Lucey P. G., Norman J. A., Crites S. T., Taylor G. J., Hawke B. R., Lemelin M., and Melosh H. J. 2014. A large spectral survey of small lunar craters: Implications for the composition of the lunar mantle. *American Mineralogist* 99:2251–2257.
- McCubbin F. M., Herd C. D. K., Yada T., Hutzler A., Calaway M. J., Allton J. H., Corrigan C. M., Fries M. D., Harrington A. D., McCoy T. J., Mitchell J. L., Regberg A. B., Righter K., Snead C. J., Tait K. T., Zolensky M. E., and Zeigler R. A. 2019. Advanced curation of astromaterials for planetary science. *Space Science Reviews* 215:48.
- McKay D., Dungan M., Morris R., and Fruland R. 1977. Grain size, petrographic, and FMR studies of the double core 60009/10: A study of soil evolution. Proceedings, 8th Lunar Science Conference. pp. 2929–2952.
- McKay D., Heiken G., and Waits G. 1978. Core 74001/2-grain size and petrology as a key to the rate of in-situ reworking and lateral transport on the lunar surface. Proceedings, 9th Lunar and Planetary Science Conference. pp. 1913–1932.
- Mitchell J., Zeigler R., McCubbin F., Needham D., Amick C., Lewis E., Graff T. G., John K. K., Naids A. J. and Lawrence S. 2020. Artemis curation: Preparing for sample return from the lunar south pole (abstract #2615). 51st Lunar and Planetary Science Conference. CD-ROM.
- Morris R. 1978a. In situ reworking (gardening) of the lunar surface—Evidence from the Apollo cores. 9th Lunar and Planetary Science Conference. pp. 1801–1811.
- Morris R. 1978b. The surface exposure (maturity) of lunar soils-some concepts and Is/FeO compilation. Proceedings, 9th Lunar and Planetary Science Conference. pp. 2287–2297.
- Noble S. K., Pieters C. M., Taylor L. A., Morris R. V., Allen C. C., McKay D. S., and Keller L. P. 2001. The optical properties of the finest fraction of lunar soil: Implications for space weathering. *Meteoritics & Planetary Science* 36:31–42.
- Noble S. K., Pieters C. M., and Keller L. P. 2007. An experimental approach to understanding the optical effects of space weathering. *Icarus* 192:629–642.
- Rose H. J., Cuttitta F., Berman S., Brown F., Carron M., Christian R., Dwornik E. J., and Greenland L. 1974. Chemical composition of rocks and soils at Taurus-Littrow. Proceedings, 5th Lunar Science Conference. pp. 1119–1133.
- Schmitt H. H., Petro N. E., Wells R. A., Robinson M. S., Weiss B. P., and Mercer C. M. 2017. Revisiting the field geology of Taurus-Littrow. *Icarus* 298:2–33.
- Shearer C., McCubbin F., Zeigler R., Gross J., Barnes J., Burgess K., Cohen B. A., Curran N., Elsila J. E., Dyar M. D., Sehlke A., Walroth R. C., Welten K. C., ANGSA Science Team, and the ANGSA Curation Team. 2020. Angsa initiative, a low-cost lunar “sample return mission.” Science and engineering goals, special samples, teams, and progress (abstract #1181). 51st Lunar and Planetary Science Conference. CD-ROM.
- Stöffler D., Knöll H. D., Marvin U. B., Simonds C. H., and Warren P. H. 1980. Recommended classification and nomenclature of lunar highland rocks—A committee report. In *Lunar highlands crust*, edited by Papike J. J. and Merrill R. B. Houston, Texas: Lunar and Planetary Institute. pp. 51–70.
- Sun L. and Lucey P. G. 2021. Unmixing mineral abundance and mg# with radiative transfer theory: Modeling and applications. *Journal of Geophysical Research: Planets* 126: e2020JE006691.
- Sun L., Lucey P. G., and Taylor G. J. 2021. Correlating Apollo soil mineralogical data with Kaguya spectral data for a global mineralogical classification. *Journal of Geophysical Research: Planets* 126:e2020JE006445.
- Taylor G. J., Martel L. M., Lucey P. G., Gillis-Davis J. J., Blake D. F., and Sarrazin P. 2019. Modal analyses of lunar soils by quantitative X-ray diffraction analysis. *Geochimica et Cosmochimica Acta* 266:17–28.
- Zeigler R., Hanna R., Edey D., Eckley S., Ketcham R., Gross J., and McCubbin F. 2020. Using X-ray computed tomography to image Apollo drive tube 73002 (abstract #3023). 51st Lunar and Planetary Science Conference. CD-ROM.